Structural instability and lattice site occupation of Mn²⁺ ions in the SrTiO₃ quantum paraelectric

V. Laguta [1] O. Laguta,[2] I. Zdeg,[2] and P. Neugebauer[2]

[1]*Institute of Physics, Czech Academy of Sciences*, Na Slovance 1999/2, 18200 Prague, Czech Republic
[2]*Brno University of Technology*, Central European Institute of Technology, Purkyňova 656/123, 61200 Brno, Czech Republic

Strontium titanate (SrTiO₃) is the most known material from the family of quantum paraelectrics. Thanks to its extremely "soft" lattice, its functionality can be easily tuned by applying both external stimuli (pressure, strain, electric field) and through doping or isotope exchange. In this paper, we present the results of a detailed study of two Mn²⁺ centers in Mn-doped SrTiO₃ single crystals using both continuous wave and pulsed electron paramagnetic resonance (EPR) spectroscopy at frequencies from 9.5 to 427 GHz and temperatures from 5 to 296 K. The first center is created by a Mn²⁺ ion at the Sr²⁺ lattice site in an off-center position. Its spectroscopic characteristics were determined for both fast and slow motion regimes of the impurity ion. In particular, all spin transitions allowed by the Mn²⁺ spin were well resolved in the slow motion regime. The second center is created by a Mn²⁺ ion at the Ti⁴⁺ position in the center of the oxygen octahedron. It has been established that the surrounding of this ion undergoes strong distortion when cooled below the phase transition temperature $T_c = 105$ K, stimulated by the rotation of the oxygen octahedron. The present data also perfectly explain the previously obtained EPR data from measurements of SrTiO₃:Mn ceramics at low microwave frequencies (9–10 GHz).

I. INTRODUCTION

SrTiO₃ is one of the most thoroughly studied ferroelectric-active materials in solid state physics. During the past two decades the topics of main interest were the quantum paraelectric behavior and quantum tunneling of local polarization [1,2], lattice dynamics and ferroelectricity in the ¹⁸O isotope enriched crystals [3,4], weak polarity at low temperatures [5], superconductivity [6], ferroelectricity induced by off-center paramagnetic dopants and corresponding magnetoelectrically coupled multiglass state [7,8], and recently possible utilization of the unique dielectric properties of SrTiO₃ in the nonvolatile electric control of spin-charge conversion in a Rashba system [9] and in spin-based quantum information systems [10]. Also, significant progress has been made in the technology of growing SrTiO₃ epitaxial films in recent years. In particular, SrTiO₃ films with the ferroelectric phase at room temperature were grown using strain engineering [11,12]. Later, topological excitations (vortex and skyrmion polar textures) were discovered in SrTiO₃ − PbTiO₃ epitaxial superlattices [13,14]. Doped by electron spins such polar superlattices offer the potential for future applications in spintronics, quantum information processing, and sensing [15,16].

Significant research effort has been focused on the characterization of the nature of Mn-related centers and ferroelectricity in Mn-doped SrTiO₃ ceramics by using both experimental techniques [7,17–23] and theoretical modeling (see, e.g., Ref. [24] and references therein). It was revealed that a strong dielectric anomaly appears around 60 K in ceramics that have been specially prepared with Mn²⁺ ions primarily substituting Sr²⁺ host ions. This anomaly is similar to that found in another quantum paraelectric, KTaO₃, which was doped by off-center Li⁺ ions [25]. Therefore, the

dielectric anomaly was reasonably attributed to hopping of the Mn²⁺ ions between off-center positions in SrTiO₃ lattice as the ionic radius of Mn²⁺ (0.96 Å) is substantially smaller than that of Sr²⁺ (1.26 Å) [26]. The Mn²⁺ off-centrality was then confirmed by electron paramagnetic resonance (EPR) [27] and extended x-ray absorption fine structure measurements [18,20,21]. The DFT-based calculations also predict the off-center position of Mn²⁺ ions [24,28–30]. However, in fact, only broadening up to complete disappearance at approximately 100 K of the motionally averaged spectrum was measured in EPR. The low-temperature EPR spectrum of Mn²⁺ at the Sr²⁺ site in the slow motion regime, where all spin transitions allowed by the spin $S = 5/2$ must be visible, was never observed. Previous measurements of ceramic samples only demonstrated broad and intensity weak "bumps" [27] which could hypothetically belong to the low-temperature Mn²⁺ spectrum. Therefore, the EPR study of Mn-doped SrTiO₃ single crystals is very desirable.

Mn²⁺ centers in SrTiO₃ single crystals were previously studied in [31]. The study identified two distinct types of Mn²⁺ centers in reduced crystals through EPR. One of the centers displayed cubic symmetry, while the other exhibited axial symmetry about one of the cubic edges. The cubic Mn²⁺ center was assigned to Mn²⁺ substitutional for Ti⁴⁺ with no local charge compensator. The second one, characterized by highly anisotropic fine structure transitions with large zero-field splitting, was assigned to the Mn²⁺ − V_O pair center. The cubic Mn²⁺ spectrum was observed only above approximately 100 K. At lower temperatures, Mn²⁺ spectral lines broadened to the extent that they were no longer observable. Upon further cooling to 4.2 K, a much more complex anisotropic spectrum appeared, which, however, was not analyzed due to weak resolution. In fact, all these features of

the cubic Mn^{2+} center described in [31] well coincide with those of Mn^{2+} center assigned to Sr site in ceramic samples, e.g., [27,20]. Given this fact and the common interest in Mn doping of $SrTiO_3$, which substantially increases the functionality of $SrTiO_3$-based materials, the previous results on Mn^{2+} centers in single crystals must be reexamined. In regard to manganese-doped ceramics, various Mn-related centers are comprehensively reviewed in publication [20].

In this paper, we present results of our detailed EPR investigation of two Mn^{2+} centers in $SrTiO_3$ created by manganese ions at both Sr and Ti sites with no local charge compensator: Mn^{2+}(Sr) and Mn^{2+}(Ti) centers, respectively. The measurements are performed on single crystals with manganese concentration ranging about 0.03–0.3 at. %. In order to diminish the dominant Mn^{4+} valence state of manganese to the desirable Mn^{2+}, the crystals were codoped by W^{6+} ions. Both the conventional continuous wave (cw) and advanced pulse EPR techniques were utilized for measurements at temperatures from 296 K down to 5 K. To simplify the Mn^{2+} spectra at low temperatures, where all spin transitions become visible, measurements were also done at very high microwave frequencies (200–427 GHz). Our results unambiguously confirm the off-center nature of Mn^{2+} when it replaces Sr^{2+} lattice ion. On the contrary, Mn^{2+} replaces Ti^{4+} at the central position in oxygen octahedron. However, it shows quite unusual behavior below the temperature of the structural phase transition at 105 K as compared to other impurities substituted for Ti (e.g., Mn^{4+}, Fe^{3+}, Cr^{3+}). In particular, high anisotropy of the Mn^{2+}(Ti) spectrum at $T < 105$ K suggests that Mn^{2+} surrounding undergoes strong distortion at the phase transition.

II. EXPERIMENT

$SrTiO_3$ crystal used in our measurements was grown by the Verneuil method [32]. In order to suppress the substitution of Mn ions at Ti site (Mn^{4+} isovalent substitution) and, thus, increase the probability for manganese penetration as Mn^{2+} ions, the crystal was grown with adding W^{6+} codopant (about 0.3 at. %). The manganese dopant was not homogeneously distributed in the volume of the boule in terms of concentration and type of centers. Therefore, by selecting a suitable part of the boule, small samples could be prepared with a dominant concentration of one or two centers of interest. In particular, one sample (no. 1) had high (about 0.3 at. %) concentration of both Mn^{2+} at Sr^{2+} site [Mn^{2+}(Sr) center] and Mn^{4+} at Ti^{4+} sites [Mn^{4+}(Ti)], the second sample (no. 2) had dominant but small concentration of Mn^{2+}(Sr) (about 0.05 at. %) and a two to three times smaller amount of Mn^{2+} at Ti sites [Mn^{2+}(Ti) center]. All these concentrations were estimated from the dipole broadening of spectral lines and their relative intensities for different centers assuming that the Sr/Ti ratio is equal to unit.

The measurements were done on small (typical size $2.0 \times 1.5 \times 0.25$ mm^3) crystal plates of rectangular shape with edges coinciding with the cubic $\langle 100 \rangle$ axes using Bruker EMX plus EPR spectrometer equipped with a low Q-factor MW resonator (Bruker 4104OR, $Q \approx 3000$) to avoid the influence of the high dielectric permittivity of $SrTiO_3$ at low temperatures (it reaches up to 25 000 even at the frequency of
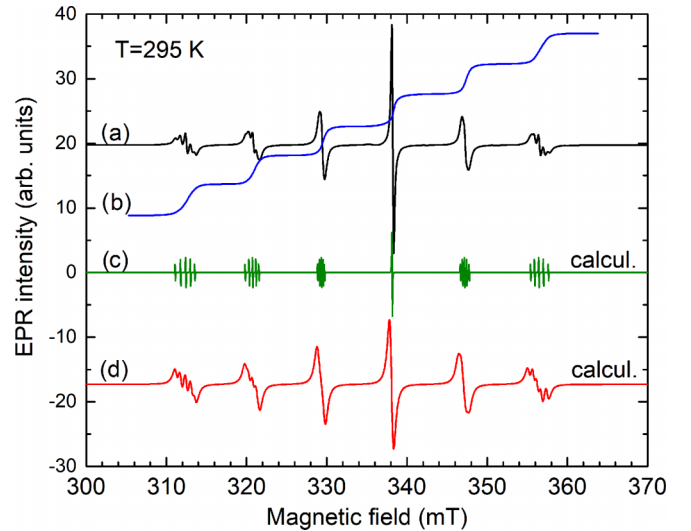

FIG. 1. Mn^{2+}(Sr) EPR spectrum measured in $SrTiO_3$ crystal (sample 2) with low manganese concentration (about 50 ppm) showing resolved five $M_S \leftrightarrow M_S - 1$ transitions for some of six HF lines (a). All HF components have the same intensity as illustrated by the double integrated spectrum (b). Spectrum (c) is the calculated spectrum in the limit of narrow lines, and spectrum (d) is the simulated spectrum.

9.5 GHz [33]). Pulse EPR measurements were carried out with the Bruker E580 spectrometer equipped with the dielectric ring MD5 resonator. For the high frequency EPR measurements (200–427 GHz), the home-made high frequency rapid scan electron spin resonance spectrometer (THz-FRASCAN-ESR) operating at frequencies up to 1 THz was utilized [34]. All three spectrometers were equipped with liquid helium cryostats allowing measurements in the temperature range 3.5–300 K.

III. EXPERIMENTAL RESULTS

A. Mn^{2+} at Sr site

The Mn^{2+} spectrum measured in sample 2 is shown in Fig. 1. Its g factor of 2.0032 and the splitting between six hyperfine components (≈ 9.2 mT) are completely the same as those measured previously for Mn^{2+} ion substituted for Sr^{2+} in ceramic samples [20,27,35]. However, due to a narrower linewidth, a specific splitting of each hyperfine line is resolved now. The spectrum is thus unusual as for a paramagnetic ion in a crystalline matter. It has all the characteristic features of a paramagnetic ion in liquid, where all anisotropic interactions of Mn^{2+} ion with its surrounding are averaged to zero. This confirms that the Mn^{2+} ion at the Sr^{2+} site indeed undergoes fast motion in the lattice in accordance with the earlier data obtained in ceramic samples [7,17,27]. The resonance fields are described by the spin Hamiltonian used for liquids:

$$\mathbf{H} = \beta_e \mathbf{S} g B + \mathbf{S} A \mathbf{I}, \quad (1)$$

where β_e is the Bohr magneton, g is the g factor, $S = 5/2$ and B are the electron spin and magnetic field, respectively, and A is the hyperfine (HF) constant of the ^{55}Mn isotope (nuclear

spin $I = 5/2$ and 100% abundance). Both the Zeeman and HF interactions are isotropic.

The splitting observed at HF lines originates from the *SAI* term in the spin Hamiltonian (1) for the spin $S \geqslant 1$. This term makes resonance fields of the $M_S \leftrightarrow M_S - 1$ fine transitions slightly different within different HF lines. Because this resonance field shift is proportional to $A^2/g\beta_e B$ (see, e.g., formulas in [36]), it is small (≈ 1 mT) even at *X*-band microwave frequencies (9–10 GHz) and is completely invisible in the *Q* microwave band (35–40 GHz) or higher frequencies. Usually, these fine transitions are broadened by random crystal fields and thus are not visible (e.g., Mn^{2+} in CaO [37]) or split by the cubic components of crystal field (for instance, Mn^{2+} ion in cubic crystal MgO [38]). In our case, all anisotropic interactions of Mn^{2+} ion with lattice (including high-order cubic terms) are averaged out by fast motion of this ion between off-center positions at the Sr site. Therefore, all the $M_S \leftrightarrow M_S - 1$ transitions related to the *SAI* term are well visible. This is also confirmed by the calculated spectra [spectra (c) and (d) in Fig. 1; energy level diagrams in the Supplemental Material [39]] performed using numerical solution of the spin Hamiltonian (1) [40]. Double integration of the complex HF lines of the measured spectrum shows that they have the same intensity [spectrum (b) in Fig. 1]. Therefore, the spectrum originates exclusively from Mn^{2+} ions at Sr^{2+} sites without marked contribution from other possible centers which could lead to the complex character of the spectrum shown in Fig. 1.

As the temperature decreases, the Mn^{2+}(Sr) spectral lines start to broaden (Fig. 2), resembling the behavior observed in the ceramic samples [27]. As a result, the spectrum is completely invisible between 20 and 120 K. At these temperatures, only the Mn^{4+} spectrum is visible [Fig. 2(b)]. However, with further temperature decrease, the Mn^{2+} spectrum appears again but with well distinguished sixsets related to the $M_S \leftrightarrow M_S - 1$ fine transitions in Fig. 2(c). This corresponds to the slow motion regime of the paramagnetic ion, when the rate of Mn^{2+} hopping between off-center positions becomes smaller than the zero-field splitting energy of the off-center shifted ion. At these low temperatures, the Mn^{2+}(Sr) spectrum is determined by the crystal field created by the off-center shifted Mn^{2+} ion and the formation of tetragonal symmetry domains with tetragonal axes pointing in either of three pseudocubic [100], [010], and [001] directions due to the phase transition in $SrTiO_3$ at $T_c = 105$ K. This leads to creation of at least three magnetically nonequivalent Mn^{2+}(Sr) centers, differing in the directions of their magnetic axes.

A similar Mn^{2+} spectrum with a resolved fine structure was measured using the echo-detected field sweep (EDFS) pulse EPR (Fig. 3). Note that the low-temperature spectrum in Fig. 2 was measured with extremely small microwave power, of only 1 μW, as microwave fields are substantially enhanced at the paramagnetic ion at temperatures 4–20 K due to the large (up to 25 000) dielectric constant of $SrTiO_3$ even at 9–10 GHz frequencies [33]. Furthermore, due to the high dielectric constant, it was challenging to measure the angular dependencies of spectra using the cw EPR technique, as it strongly influenced the tuning of the EPR resonator. Therefore, the pulse EPR technique was applied to measure angular dependencies of the Mn^{2+} spectrum. However, as it can be seen from Fig. 3, the angular variation of the Mn^{2+} spectrum
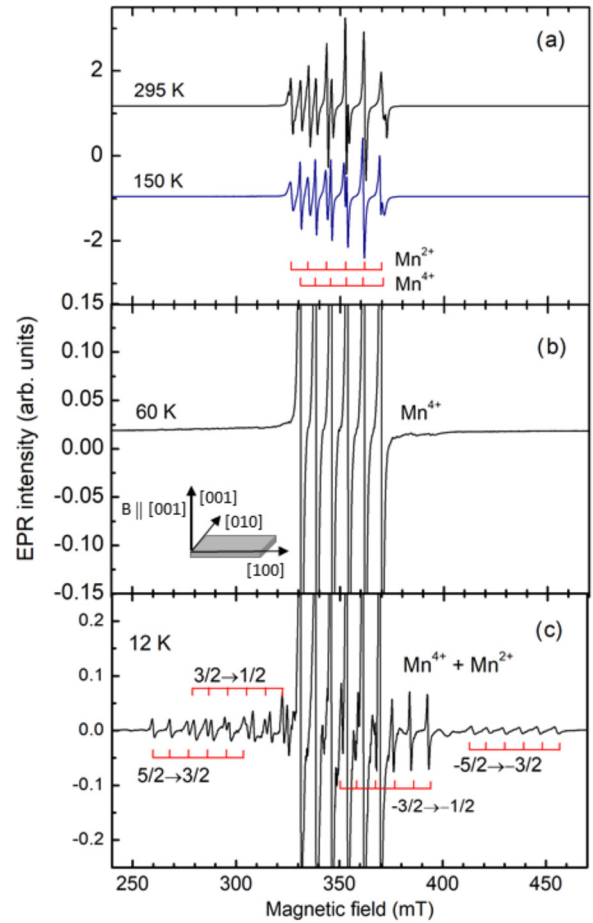

FIG. 2. Mn^{2+}(Sr) and Mn^{4+}(Ti) EPR spectra measured in $SrTiO_3$:Mn,W crystal (sample 1) at temperatures 295 and 150 K (a), 60 K (b), and 12 K (c). The spectra at 60 and 12 K are shown with a magnification factor of 10. Also, due to the strong saturation effects in spin transitions at low temperatures, the microwave power for the spectrum taken at 12 K was only 1 μW. The most visible spin transitions are labeled in (c); they correspond to the magnetic field direction perpendicular to the tetragonal axis, directed in either of the two pseudocubic [100] and [010] directions, as shown in the inset to (b).

is quite complex due to the immense number of spin transitions (there are 90 spectral lines for allowed transitions only, taking into account the presence of, at least, three magnetically inequivalent Mn^{2+} centers) and small splitting between $M_S \to M_S - 1$ sixsets. Additional difficulties arise also from the contribution of forbidden transitions when the magnetic field deviates from the symmetrical orientation along [001] cubic axis and the contribution of the intense Mn^{4+} spectrum. The forbidden transitions are presented even at [001] magnetic field orientation as two of the three Mn^{2+} centers have magnetic axes perpendicular to the magnetic field. This difficulty was resolved by performing measurements at 210 GHz frequency.

The spectra measured at 210 GHz are shown in Fig. 4. In contrast to the measurement at 9.5–9.8 GHz, at this high frequency, the central transition Mn^{2+} sixset is not broadened by motion of paramagnetic ion as it is not affected by crystal fields (it is insensitive to crystal fields) as the second order
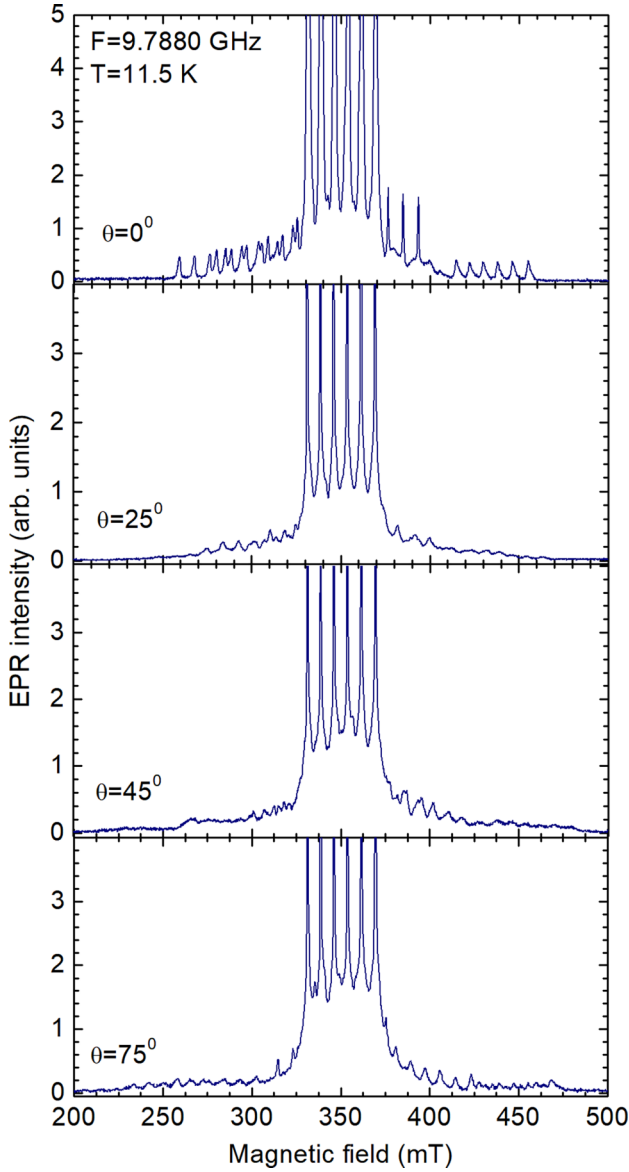
FIG. 4. Mn^{2+}(Sr) and Mn^{4+}(Ti) EPR spectra measured in sample 1 at 210 GHz and magnetic field orientation along [001] pseudocubic direction (see inset in Fig. 2). Simulated spectrum (in red) shows the most intensive Mn^{2+} sixsets related to the $M_S \leftrightarrow M_S - 1$ transitions that were calculated considering the populations of the energy levels at 11 K. The "∥" and "⊥" symbols denote the magnetic field direction along or perpendicular to tetragonal magnetic axis (see the inset to Fig. 2).

FIG. 3. Angular variation of the Mn^{2+}(Sr) and Mn^{4+}(Ti) EDFS EPR spectra in $SrTiO_3$:Mn,W crystal (sample 1) showing resolved $M_S \leftrightarrow M_S - 1$ transitions for Mn^{2+}(Sr) ion, similar as in Fig. 2.

shifts of this transition by crystal fields are zero. Also, at such high frequency and, respectively, high magnetic fields (7.3–7.7 T) Mn^{4+} and Mn^{2+} sixsets are well separated from each other even for the small difference in their g factors, 1.994 and 2.003, respectively (Table I). Similar to measurements at low microwave frequency, the $M_S \leftrightarrow M_S - 1$ transitions become visible at 6–15 K. At this low temperature, the Mn^{2+} spectrum can be described by the spin Hamiltonian for a static ion in a crystalline matter. It has the following form:

$$\mathbf{H} = g\beta\mathbf{BS} + D\left(\mathbf{S}_z^2 - \tfrac{1}{3}S(S+1)\right) + E\left(\mathbf{S}_x^2 - \mathbf{S}_y^2\right) + \mathbf{SAI},$$

(2)

where D and E are the zero-field splitting parameters. The fourth order cubic terms of crystal field for the spin $S = 5/2$ are omitted. They are negligibly small compared to the D- and
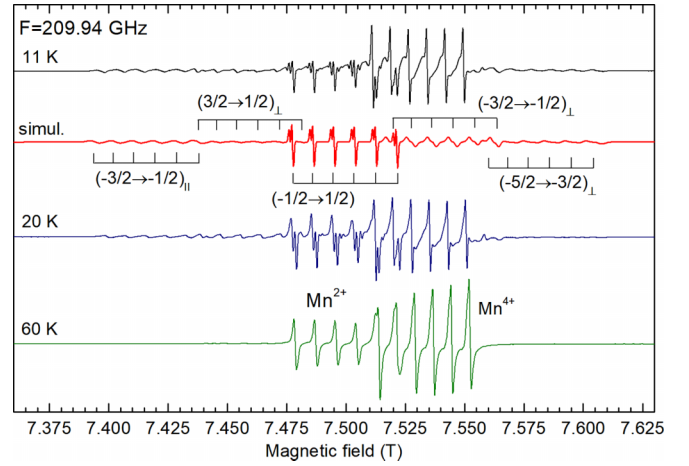
E-contained terms in the spin Hamiltonian, as there is no shift of the Mn^{2+} spectral lines in the cubic phase at $T > T_c$.

The spin Hamiltonian parameters were obtained from the fitting of the measured spectrum at $B \parallel [001]$ to the calculated one (Fig. 4, spectrum in red). The presence of two types of centers with magnetic axes parallel and perpendicular to magnetic field allows for easy determination of spin Hamiltonian parameters. This gives $g = 2.0032$, $A = 246$ MHz, $D = -1150$ MHz, and $E = 9$ MHz. Note that the $M_S \leftrightarrow M_S - 1$ transitions were calculated taking into account the populations of the energy levels at 11 K. The visible transitions are classified in the simulated spectrum according to the energy levels of spins at $B \parallel [001]$. Since the difference in the energy levels population at the magnetic field of 7.5 T is large, some transitions are not visible at all. There is also a small splitting of the $1/2 \leftrightarrow -1/2$ central transition due to small anisotropy of the g factor, $\Delta g \approx 0.0004$. Although the Mn^{2+} center has nearly axial symmetry along the [100] cubic direction, the weak rhombicity parameter E included in the fit model clearly improves the fitting of the measured spectra as the spectral lines of all the fine transitions are markedly split. This means that there is a superposition of the strong tetragonal field characteristic for the Sr lattice site (see, e.g., Gd^{3+} parameters in Table I and ^{87}Sr NMR data [41]) and the field created by the off-center Mn^{2+} ion, which could be shifted not exactly along the simple ⟨100⟩ cubic directions. Our experiment cannot distinguish these two contributions because the low temperature "static" Mn^{2+} spectrum becomes visible only at $T \ll T_c = 105$ K. In general, one can expect strong influence of the phase transition on Mn^{2+} dynamics as the shifts of oxygen ions with respect to the Sr site at phase transition are sizable, d(Sr-O) = 2.712 and 2.810 Å, at $T < 10$ K. Of course, due to the size mismatch between Sr and Mn, the Mn surrounding ions undergo much larger shifts

TABLE I. EPR parameters for Mn^{4+} and Mn^{2+} ions in $SrTiO_3$. For comparison, EPR parameters of Fe^{3+} and Gd^{3+} ions in $SrTiO_3$ are listed as well. The crystal field parameters b_n^m and HF splitting constant A are given in MHz units.

Center	g factor	$b_2^0 = D$	$b_2^2 = 3E$	b_4^0	b_4^4	A	T (K)	Refs.
Mn^{4+}(Ti)	1.994(1)	0	0			209(3)	296	[51]
	1.994(1)	2.94	0			209(3)	77	[51]
Mn^{2+}(Sr)	2.0032(2)	0		≈ 0	≈ 0	248(1)	296	[27,20,35,52]
	2.0032(2)[a]	−1150(10)	27(3)	≈ 0	≈ 0	246(1)	11	this work
Mn^{2+}(Ti)	2.0013(1)	0	0	≈ 0	≈ 0	238(1)	105	this work[b]
	2.0013(2)	−335(2)	40	≈ 0	≈ 0	238(1)	24	this work
Fe^{3+}(Ti)	2.004(1)	0	0	330	1650		105	[53]
	2.0037(5)	34	0		1700		4.2	[44]
Gd^{3+}(Sr)	1.992(2)	0	0	−17.1(6)			300	[45]
	1.992(2)	1087(2)	0	−9.7(2)	−12.6(2)		4.2	[45]

[a]At temperatures 10–20 K, g factor shows weak anisotropy $\Delta g \approx 0.0004$ revealed in measurements at the microwave frequency 210 GHz.
[b]Similar Mn^{2+} spectrum was measured in the reduced $SrTiO_3$:Mn ceramics at room temperature [35].

than those expected for the centrosymmetric Mn position (see, e.g., Table 2 in Ref. [20] and Table I in Ref. [24]). The theoretical calculations [20,24,42] predict various possible local geometries for Mn^{2+} center which are, however, sensitive to input parameters and model of calculation. In particular, the best-fit model presented in [20] suggests deviations of the Mn off-centering from the cubic axes with the resulting symmetry of the Mn^{2+}(Sr) center being reduced to monocliniclike that obviously agrees with our data.

B. Mn^{2+} at Ti site

Besides the Mn^{2+} spectrum shown in Fig. 1, another Mn^{2+} spectrum (assigned below as Mn^{2+} at Ti site) was observed as well in sample 2 (Fig. 5).
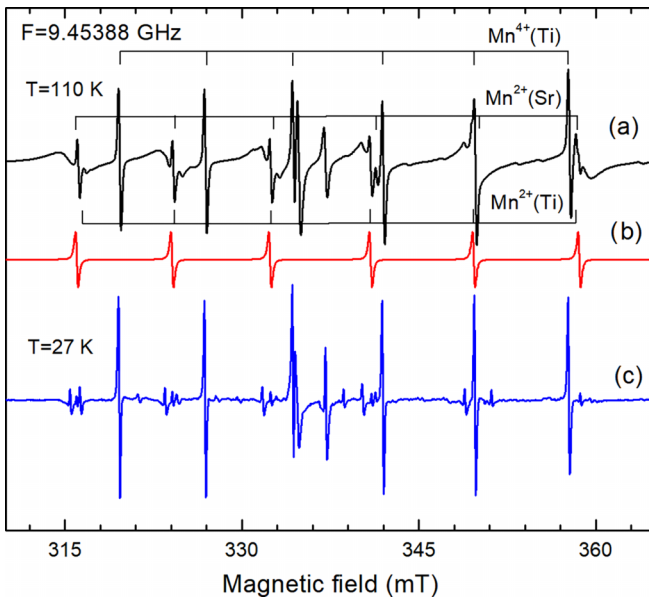

FIG. 5. (a),(c) EPR spectra measured in $SrTiO_3$:Mn crystal (sample 2) at 110 and 27 K, respectively, showing six broad HF lines from Mn^{2+} at Sr site, six intense HF lines from Mn^{4+} at Ti site, and six narrow HF lines from Mn^{2+} at Ti site [its simulated spectrum is shown separately in (b)].

The spectrum contains only the central $1/2 \leftrightarrow -1/2$ electron spin transition split into six ^{55}Mn HF components. Other electron spin transitions are not visible due to broadening by inhomogeneity of crystal fields and small values of high-order cubic terms, suggesting that there is no motion of the Mn^{2+} ion. This Mn^{2+} spectrum is completely isotropic, similar to the Mn^{4+} spectrum (angular dependencies are presented in Figs. S2 and S3 in the Supplemental Material [39]). It has thus cubic symmetry and is described by g factor 2.0013 and the HF constant $A = 238$ MHz; both are typical for a Mn^{2+} ion in the oxygen octahedron. A corresponding simulated spectrum is shown in Fig. 5 as well [spectrum (b)]. It means that this Mn^{2+} ion is substituted for Ti^{4+} with charge compensation far from the paramagnetic ion. Obviously, this is the same Mn^{2+} center reported in [35] for SrO-rich $SrTiO_3$ ceramics. As the temperature decreases, Mn^{2+}(Ti) spectral lines do not broaden like Mn^{2+}(Sr) ones. However, below the phase transition at 105 K, each Mn^{2+} HF line splits into a few components [spectrum (c) in Fig. 5]. A more detailed temperature dependence of the Mn^{2+} spectrum is shown in Fig. 6.

At arbitrary orientation of magnetic field with respect to crystal axes, the spectrum contains four visible spectral components whose resonance fields change when the magnetic field rotates around the [001] cubic axis (Fig. S2 in the Supplemental Material [39]). However, the angular dependencies of the resonance fields were not quantitatively analyzed, as the shift of spectral lines is weak (for the central transition, it is a second order effect of crystal field change). Besides, the crystal below the phase transition temperature becomes multidomain (the symmetry changes from the cubic $m3m$ to the tetragonal $I4/mcm$ with the tetragonal axis pointed along any of the ⟨100⟩ pseudocubic directions). This additionally complicates the spectrum.

The spin Hamiltonian parameters of the Mn^{2+}(Ti) center were calculated using the spin Hamiltonian (2). The spectra were simulated for $B \parallel [001]$, where the splitting is largest. This means that the magnetic z axis is oriented at any of the three ⟨100⟩ directions. The other two magnetic axes defined by the E terms in the spin Hamiltonian (2) are located in the perpendicular plane. Because the x and y magnetic axes are interchangeable, overall, there should be six magnetically inequivalent centers with orthorhombic symmetry. But not
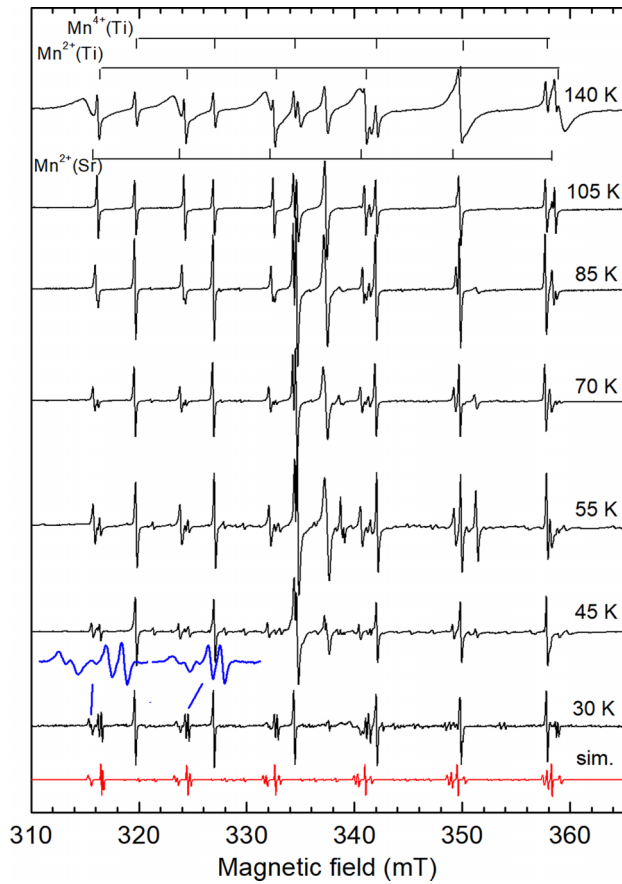
FIG. 6. Temperature dependence of EPR spectra in the same crystal as in Fig. 5 at the magnetic field orientation $B \parallel [001]$. The last spectrum at 30 K was measured at the magnetic field orientation deviated by $\approx 15°$ from [001] direction to show the splitting of the Mn^{2+}(Ti) HF components into four lines due to structural phase transition at 105 K. Its simulated spectrum is shown in red.

FIG. 7. Temperature dependence of the crystal field parameter D for the Mn^{2+}(Ti) center in $SrTiO_3$ crystal. Solid red line presents the theoretical fit according to Eq. (3).

all centers are distinguished separately for the $1/2 \leftrightarrow -1/2$ central transition. In this relation, the angular variation of the Mn^{2+} spectrum is very similar to that of the $Fe^{3+} - V_O$ center described in detail in [43]. The rhombicity of the Mn^{2+} center, as in the case of $Fe^{3+} - V_O$ center, is related to rotation of the oxygen octahedron at the phase transition. As an example, the last spectrum in Fig. 6 measured at 30 K was simulated (shown in red) with the following parameters: $g = 2.0013$, $D = -330$ MHz, $E = 13$ MHz, and $A = 238$ MHz. The temperature dependence of the axial crystal field component D is shown in Fig. 7.

Excepting temperatures just below the phase transition temperature, where the D values can be determined only roughly, the temperature dependence of the D constant can be described by the function

$$D(T) \propto (T_c - T)^{0.5}, \qquad (3)$$

i.e., $D(T) \propto \varphi$, where φ is the order parameter of the phase transition (rotation angle of oxygen octahedron). This functional dependence of the crystal field parameter D is similar to that found in $SrTiO_3$ for Fe^{3+} and Gd^{3+} ions [44,45]. If we compare the D constant values with those for Mn^{4+} and Fe^{3+} ions substituted for Ti as well (Table I), one can notice that the
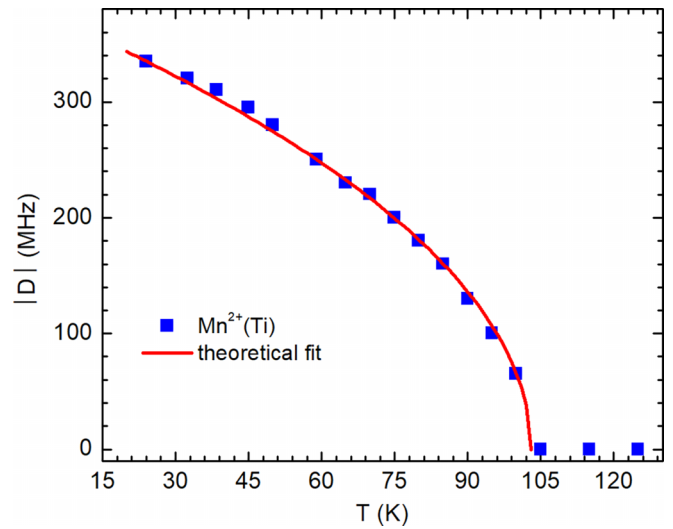
D constant for Mn^{2+} ions is about 10 and 100 times larger than that for Fe^{3+} and Mn^{4+}, respectively (Table I). For instance, one can see from Figs. 5 and 6 that Mn^{4+} spectral lines are not visibly split even at the temperature 27–30 K. This reflects unusual behavior of Mn^{2+} ion whose D constant is usually much less than that of Fe^{3+} in the same crystal fields (see, e.g., tables with spin Hamiltonian parameters in [46]). The cubic crystal field parameter b_4^4 for Mn^{2+} is also negligibly small compared to 1650–1700 MHz for Fe^{3+}. This fact suggests the possibility of the Mn^{2+} ion displacement from its position at the center of oxygen octahedron or distortion of surroundings of this ion stimulated by rotation of oxygen octahedron at $T < T_c$. The last option seems to be more probable as the Mn^{2+} ion is larger than Ti^{4+}: ionic radii are 0.83 and 0.605 Å, respectively [26]. This exciting experimental result in $SrTiO_3$ is interesting because, apart from oxygen ions, other host ions and all known dopants at the Ti site (Mn^{4+}, Fe^{3+}, Cr^{3+}) do not shift at the phase transition. The oxygen octahedron is also not distorted in the low-temperature phase. On the other hand, the V^{4+} and Cr^{5+} centers (both ions replace Ti^{4+}) undergo a Jahn-Teller distortion [47,48]. The behavior of their spectra with cooling is the same as for the Mn^{2+}(Ti) center. However, this is not the case, since Mn^{2+} is not a Jahn-Teller ion. Clearly, this finding requires further theoretical explanation.

Let us compare the present results on Mn^{2+} centers in $SrTiO_3$ with those published in early works by Muller *et al.* in single crystals [31] and other authors in Mn-doped ceramics, e.g., Refs. [49,50]. It is completely clear that the cubic Mn^{2+} spectrum described in [31] corresponds to the Mn^{2+} at Sr site as was already noted in [35,20]. Due to the highly anisotropic character of both the Mn^{2+}(Ti) and Mn^{2+}(Sr) centers in the low-temperature phase of $SrTiO_3$ (see, e.g., the parameters of spin Hamiltonian presented in Table I), their EPR spectra in ceramics are spread over a broad range of magnetic fields by random distribution of crystallite axes, including even the central transition $-1/2 \rightarrow 1/2$, which is significantly
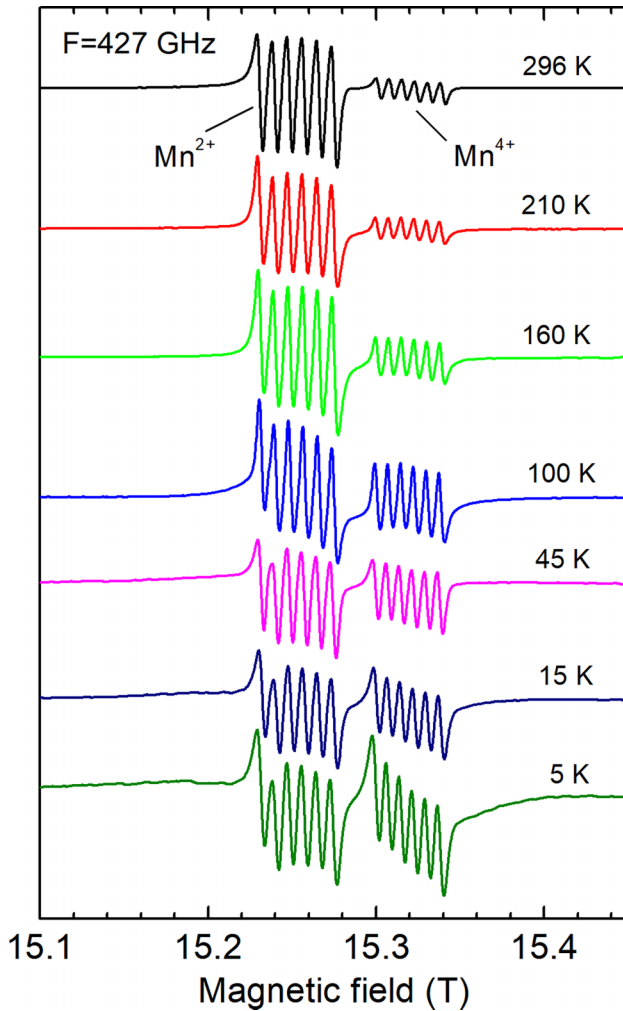
FIG. 8. Temperature dependence of $Mn^{2+}(Sr)$ and $Mn^{4+}(Ti)$ EPR spectra in $SrTiO_3$:2 mol % Mn ceramics measured at 427 GHz. The central transition sixsets of Mn^{2+} and Mn^{4+} ions are well seen to the lowest temperature of 5 K. Below approximately 45 K, a broad characteristic spectrum of the $M_S \leftrightarrow M_S - 1$ transitions of $Mn^{2+}(Sr)$ center appear.

broadened by second order effects from crystal fields. This makes the Mn^{2+} spectra in ceramics invisible at $T < 105$ K, except for measurements at high microwave frequencies, where the second-order effects are zero and the central transition lines of Mn^{2+} and Mn^{4+} ions are well separated from each other. This explains well the earlier EPR data in ceramic samples [49,50]. In particular, the disappearance of Mn^{2+} spectra at $T < 105$ K previously explained in [49] as due to the $Mn^{2+} \rightarrow Mn^{3+}$ recharge, in reality comes from the abrupt broadening of spectral lines (even of the central transition) with temperature lowering, when measurements are done at low microwave frequencies. As can be seen from our measurements at high microwave frequency (427 GHz, Fig. 8), the central transition sixset of $Mn^{2+}(Sr)$ center is well observable to the lowest temperatures without change of the Mn^{2+}/Mn^{4+} ratio. A small variation in the spectral intensities is only caused by different broadening of Mn^{2+}/Mn^{4+} spectral lines with temperature decrease. Moreover, below approximately 45 K, a broad characteristic feature related

to the $M_S \rightarrow M_S - 1$ fine transitions of the $Mn^{2+}(Sr)$ center appears. The resonance fields of these transitions are spread out by the random distribution of crystallite axes leading thus to the strong broadening of the spectral lines.

IV. CONCLUSIONS

Two Mn^{2+} centers, originating from manganese ions in $SrTiO_3$ single crystals, were investigated by EPR at temperatures from 296 K down to 5 K and microwave frequencies extending to 427 GHz. Both the continuous wave and pulse EPR techniques were utilized.

The first center is formed by Mn^{2+} at the Sr^{2+} lattice site in an off-center position. This is confirmed by measurements around room temperature in the fast motion regime of the impurity ion, as well as at low temperatures (below approximately 20 K) in the slow motion regime of the Mn^{2+} ion, where all spin transitions allowed by the spin $S = 5/2$ were well resolved. These transitions are seen even in the fast motion regime as a weak splitting of each of six hyperfine lines of the Mn^{2+} ion into five components due to the second-order effects in spin transitions. This splitting is proportional to the $A^2/g\beta B$ ratio and, thus, disappears at high microwave frequencies/high magnetic fields. The $Mn^{2+}(Sr)$ center has nearly axial symmetry in either of the three pseudocubic [100], [010], and [001] directions with weak rhombicity. It is characterized by the zero-field interaction parameters $D = -1150$ MHz and $E = 9$ MHz at $T = 11$ K. However, the exact direction of Mn^{2+} off-center displacement could not be determined from our measurements. This is primarily due to the superposition of the strong tetragonal field characteristic for the Sr lattice site and the field created by the Mn^{2+} off-center ion which occurs in the low-temperature tetragonal phase. The most recent theoretical calculations [20,24] suggest deviations of the Mn off-centering from the cubic axes. One can also expect a strong influence of the phase transition on Mn^{2+} dynamics as the temperature-dependent shifts of oxygen ions with respect to the Sr site are comparable to Mn^{2+} off-center shift.

The second manganese center is created by Mn^{2+} at the Ti site. In this center, the Mn^{2+} ion replaces Ti^{4+} at the central position in the oxygen octahedron without charge compensation in its nearest surroundings. The center has thus pure cubic symmetry in the cubic phase of $SrTiO_3$. Its EPR spectrum is described by the following spin Hamiltonian parameters: $g = 2.0013$, $A = 238$ MHz. The electron-nuclear coupling constant A has a typical value for Mn^{2+} in the perovskite B site supporting thus the Ti substitution. When the temperature decreases below the phase transition temperature, the symmetry of the $Mn^{2+}(Ti)$ center lowers down to the orthorhombic one, leading to strong temperature dependence of the spin Hamiltonian parameters. In particular, the D constant responsible for the axial component of the crystal field increases proportionally to the order parameter of the phase transition (rotation angle of oxygen octahedron). It reaches huge values of 335–340 MHz at $T = 24$ K as for a paramagnetic ion in the Ti site of $SrTiO_3$. This suggests strong distortion of the Mn^{2+} surroundings stimulated by rotation of oxygen octahedron at $T < T_c$.

Finally, our study provides a comprehensive understanding of the earlier EPR data obtained on $SrTiO_3$:Mn ceramic

samples at 9–10 GHz [49,50] where $Mn^{2+} \rightarrow Mn^{3+}$ recharge at the phase transition was assumed. Our measurements of $SrTiO_3$:Mn ceramics at high microwave frequency (427 GHz) did not reveal any change in the Mn^{2+} concentration upon change of temperature from 296 to 5 K. The Mn^{2+} EPR spectrum in ceramics becomes invisible below approximately 105 K at low microwave frequencies simply due to the strong broadening even of central transition lines.

[1] K. A. Muller, W. Berlinger, and E. Tosatti, Indication for a novel phase in the quantum paraelectric regime of $SrTiO_3$, Z. Phys. B: Condens. Matter **84**, 277 (1991).

[2] V. V. Lemanov, A. V. Sotnikov, E. P. Smirnova, and M. Weihnacht, Dielectric relaxation in doped $SrTiO_3$: Transition from classical thermal activation to quantum tunneling, J. Appl. Phys. **98**, 056102 (2005).

[3] M. Itoh, R. Wang, Y. Inamura, T. Yamaguchi, Y-J. Shan, and T. Nakamura, Ferroelectricity induced by oxygen isotope exchange in strontium titanate perovskite, Phys. Rev. Lett. **82**, 3540 (1999).

[4] R. Blinc, B. Zalar, V. V. Laguta, and M. Itoh, Order-disorder component in the phase transition mechanism of ^{18}O enriched strontium titanate, Phys. Rev. Lett. **94**, 147601 (2005).

[5] E. K. H. Salje, O. Aktas, M. A. Carpenter, V. V. Laguta, and J. F. Scott, Domains within domains and walls within walls: Evidence for polar domains in cryogenic $SrTiO_3$, Phys. Rev. Lett. **111**, 247603 (2013).

[6] K. Ahadi, L. Galletti, Y. Li, S. Salmani-Rezaie, W. Wu, and S. Stemmer, Enhancing superconductivity in $SrTiO_3$ films with strain, Sci. Adv. **5**, 0120 (2019).

[7] A. Tkach, P. M. Vilarinho, and A. L. Kholkin, Polar behavior in Mn-doped $SrTiO_3$ ceramics, Appl. Phys. Lett. **86**, 172902 (2005); Structure–microstructure–dielectric tunability relationship in Mn-doped strontium titanate ceramics, Acta Mater. **53**, 5061 (2005).

[8] V. V. Shvartsman, S. Bedanta, P. Borisov, W. Kleeman, A. Tkach, and P. M. Vilarinho, $(Sr,Mn)TiO_3$: A magnetoelectric multiglass, Phys. Rev. Lett. **101**, 165704 (2008).

[9] P. Noel, F. Trier, L. M. Vicente Arche, J. Brehin, D. C. Vaz, V. Garcia, S. Fusil, A. Barthelemy, L. Vila, M. Bibes, and J.-P. Attane, Non-volatile electric control of spin-charge conversion in a $SrTiO_3$ Rashba system, Nature (London) **580**, 483 (2020).

[10] F. Giustino, J. H. Lee, F. Trier, M. Bibes, S. M. Winter, R. Valenti, Y.-W. Son, L. Taillefer, Ch. Heil, A. I. Figueroa *et al.*, The 2021 quantum materials roadmap, J. Phys. Mater. **3**, 042006 (2020).

[11] J. H. Haeni, P. Irvin, W. Chang, R. Uecker, P. Reiche, Y. L. Li, S. Choudhury, W. Tian, M. E. Hawley, B. Craigo *et al.*, Room-temperature ferroelectricity in strained $SrTiO_3$, Nature (London) **430**, 758 (2004).

[12] R. Xu, J. Huang, E. S. Barnard, S. S. Hong, P. Singh, Ed. K. Wong, Th. Jansen, V. Harbola, J. Xiao, B. Y. Wang *et al.*, Strain-induced room-temperature ferroelectricity in $SrTiO_3$ membranes, Nat. Commun. **11**, 3141 (2020).

[13] A. K. Yadav, C. T. Nelson, S. L. Hsu, Z. Hong, J. D. Clarkson, C. M. Schleputz, A. R. Damodaran, P. Shafer, E. Arenholz, L. R. Dedon *et al.*, Observation of polar vortices in oxide superlattices, Nature (London) **530**, 198 (2016).

[14] S. Das, Y. L. Tang, Z. Hong, M. A. P. Goncalves, M. R. McCarter, C. Klewe, K. X. Nguyen, F. Gomez-Ortiz, P. Shafer, E. Arenholz *et al.*, Observation of room-temperature polar skyrmions, Nature (London) **568**, 368 (2019).

[15] S. E. Crawford, R. A. Shugayev, H. P. Paudel, P. Lu, M. Syamlal, P. R. Ohodnicki, B. Chorpening, R. Gentry, and Y. Duan, Quantum sensing for energy applications: Review and perspectives, Adv. Quantum Technol. **4**, 2100049 (2021).

[16] S. Das, V. Laguta, K. Inzani, W. Huang, J. Liu, R. Chatterjee, M. R. McCarter, S. Susarla, A. Ardavan, J. Junquera, S. M. Griffin, and R. Ramesh, Inherent spin-polarization coupling in a magnetoelectric vortex, Nano Lett. **22**, 3976 (2022).

[17] A. Tkach, P. M. Vilarinho, A. L. Kholkin, A. Pashkin, S. Veljko, and J. Petzelt, Broad-band dielectric spectroscopy analysis of relaxation dynamics in Mn-doped $SrTiO_3$ ceramics, Phys. Rev. B **73**, 104113 (2006).

[18] I. Levin, V. Krayzman J. C. Woicik, A. Tkach, and P. M. Vilarinho, X-ray absorption fine structure studies of Mn coordination in doped perovskite $SrTiO_3$, Appl. Phys. Lett. **96**, 052904 (2010).

[19] M. V. Talanov, A. I. Stash, S. A. Ivanov, E. S. Zhukova, B. P. Gorshunov, B. M. Nekrasov, V. S. Stolyarov, V. I. Kozlov, M. Savinov, and A. A. Bush, Octahedra-tilted control of displacement disorder and dielectric relaxation in Mn-doped $SrTiO_3$ single crystals, J. Phys. Chem. Lett. **13**, 11720 (2022).

[20] R. A. Maier, E. Cockayne, M. Donohue, G. Cibin, and I. Levin, Substitutional mechanisms and structural relaxations for manganese in $SrTiO_3$: Bridging the concentration gap for point-defect metrology, Chem. Mater. **32**, 4651 (2020).

[21] M. Valant, T. Kolodiazhnyi, I. Arcon, F. Aguesse, A.-K. Axelsson, and N. M. Alford, Origin of magnetism in Mn-doped $SrTiO_3$, Adv. Funct. Mater. **22**, 2114 (2012).

[22] R. O. Kuzian, V. V. Laguta, A.-M. Dare, I. V. Kondakova, M. Marysko, L. Raymond, E. P. Garmash, V. N. Pavlikov, A. Tkach, and P. M. Vilarinho, Mechanism of magnetoelectricity in manganese-doped incipient ferroelectrics, Europhys. Lett. **92**, 17007 (2010).

[23] D. V. Azamat, A. Dejneka, J. Lancok, V. A. Trepakov, L. Jastrabik, and A. G. Badalyan, Electron paramagnetic resonance studies of manganese centers in $SrTiO_3$: Non-Kramers Mn^{3+} ions and spin-spin coupled Mn^{4+} dimers, J. Appl. Phys. **111**, 104119 (2012).

[24] C. M. Repa and L. A. Fredin, Mn environment in doped $SrTiO_3$ revealed by first-principles calculation of hyperfine splittings, Appl. Phys. Lett. **121**, 022401 (2022).

[25] U. T. Hochli, K. K. Knorr, and A. Loidl, Orientational glasses, Adv. Phys. **51**, 589 (2002).

[26] R. D. Shannon, Revised effectice ionic radii and systematic studies of interatomic distances in halides

and chalcogenides, Acta Crystallogr., Sect. A **32**, 751 (1976).

[27] V. V. Laguta, I. V. Kondakova, I. P. Bykov, M. D. Glinchuk, A. Tkach, P. M. Vilarinho, and L. Jastrabik, Electron spin resonance investigation of Mn^{2+} ions and their dynamics in Mn-doped $SrTiO_3$, Phys. Rev. B **76**, 054104 (2007).

[28] I. V. Kondakova, R. O. Kuzian, L. Raymond, R. Hayn, and V. V. Laguta, Evidence for impurity-induced polar state in $Sr_{1-x}Mn_xTiO_3$ from density functional calculations, Phys. Rev. B **79**, 134117 (2009).

[29] I. Fongkaew, J. T. Thienprasert, and S. Limpijumnong, Identification of Mn site in Mn-doped $SrTiO_3$: First principles study, Ceram. Int. **43**, S381 (2017).

[30] X.-L. Dong, K.-H. Zhang, and M.-X. Xu, First-principles study of electronic structure and magnetic properties of $SrTi_{1-x}M_xO_3$ (M = Cr, Mn, Fe, Co, or Ni), Front. Phys. **13**, 137106 (2018).

[31] R. A. Serway, W. Berlinger, K. A. Muller, and R. W. Collins, Electron paramagnetic resonance of three manganese centers in reduced $SrTiO_3$, Phys. Rev. B **16**, 4761 (1977).

[32] Y. Tateno, K. Endo, S. Arisawa, A.-M. Vlaicu, L. Nedelcu, N. Preda, M. Secu, R. Iordanescu, A. C. Kuncser, and P. Badica, Grown of $SrTiO_3$ single crystals with diameter of about 30 mm by the Verneuil method, Cryst. Growth Des. **19**, 604 (2019).

[33] V. Laguta, V. Bovtun, M. Kempa, O. Laguta, P. Neugebauer, M. Simenas, J. Banys, and S. Kamba, Enhancement of microwave fields in pulse EPR of quantum paraelectrics, Appl. Phys. Lett. **123**, 214001 (2023).

[34] O. Laguta, A. Sojka, A. Marko, and P. Neugebauer, Rapis scan ESR: A versatile tool for the spin relaxation studies at (sub)THz frequencies, Appl. Phys. Lett. **120**, 120502, (2022).

[35] R. A. Maier, A. C. Johnston-Peck, and M. P. Donohue, (Magic dopant) amphoteric behavior of a redox-active transition metal ion in a perovskite lattice: New insights on the lattice site occupation of manganese in $SrTiO_3$, Adv. Funct. Mater. **26**, 8325 (2016).

[36] A. Abragam and B. Bleaney, *Electron Paramagnetic Resonance of Transition Ions* (Clarendon, Oxford, 1970).

[37] D. H. Tanimoto and J. C. Kemp, Forbidden hyperfine transitions in the electron spin resonance of Mn^{2+} in CaO and SrO crystals, J. Phys. Chem. Solids **27**, 887 (1966).

[38] F. Chiarini, M. Martinelli, and G. Ranieri, EPR many-quantum transitions of Mn^{2+} in MgO, J. Magn. Reson. **14**, 60 (1974).

[39] See Supplemental Material at http://link.aps.org/supplemental/10.1103/PhysRevB.110.024114 for the energy levels diagrams of the Mn^{2+}(Sr) center, and the angular dependencies of the Mn^{2+}(Ti) and Mn^{4+}(Ti) EPR spectra. The Supplemental Material also contains Ref. [40].

[40] S. Stoll and A. Schweiger, EasySpin, a comprehensive software package for spectral simulation and analysis in EPR, J. Magn. Reson. **178**, 42 (2006).

[41] V. V. Laguta, R. Blinc, M. Itoh, J. Seliger, and B. Zalar, ^{87}Sr NMR of phase transitions in $SrTi^{16}O_3$ and $SrTi^{18}O_3$, Phys. Rev. B **72**, 214117 (2005).

[42] O. E. Kvyatkovskii, *Ab initio* calculations of the geometry and electronic structure of point defects in ferroelectrics with a perovskite structure, Phys. Solid State **51**, 982 (2009).

[43] Th. Von Waldkirch, K. A. Muller, and W. Berlinger, Analysis of the Fe^{3+} - V_O center in the tetragonal phase of $SrTiO_3$, Phys. Rev. B **5**, 4324 (1972).

[44] H. Unoki and T. Sakudo, Electron spin resonance of Fe^{3+} in $SrTiO_3$ with special reference to the 110 K phase transition, J. Phys. Soc. Jpn. **23**, 546 (1967).

[45] L. Rimai and G. A. deMars, Electron paramagnetic resonance of trivalent gadolinium ions in strontium and barium titanates, Phys. Rev. **127**, 702 (1962).

[46] *Handbook of Electron Spin Resonance*, Vol. 2, edited by Ch. P. Poole and H. A. Farach (Springer-Verlag, New York, 1999).

[47] Th. W. Kool and M. Glasbeek, Electric field effects in EPR of the $SrTiO_3$:V^{4+} Jahn-Teller system, J. Phys.: Condens. Matter **3**, 9747 (1991).

[48] K. A. Muller, K. W. Blazey, and Th. W. Kool, Tetrahedral coordinated Cr^{5+} in $SrTiO_3$, Solid State Commun. **85**, 381 (1993).

[49] T. R. N. Kutty, L. Gomathi Devi, and P. Murugaraj, The change in oxidation state of Mn ions in semiconducting $BaTiO_3$ and $SrTiO_3$ around the phase transition temperatures, Mat. Res. Bull. **21**, 1093 (1986).

[50] C. B. Azzoni, M. C. Mozzati, A. Paleari, V. Massarotti, M. Bini, and D. Capsoni, Magnetic evidence of different environments of manganese ions in Mn-substituted strontium titanate, Solid State Commun. **114**, 617 (2000).

[51] K. A. Muller, Electron paramagnetic resonance of manganese IV in $SrTiO_3$, Phys. Rev. Lett. **2**, 341 (1959).

[52] A. Zorko, M. Predeli, H. Luetkens, A.-K. Axelsson, and M. Valant, Intrinsic paramagnetism and aggregation of manganese dopants in $SrTiO_3$, Phys. Rev. B **89**, 094418 (2014).

[53] K. A. Muller, Paramagnetische rezonanz von Fe^{3+} in $SrTiO_3$ einkristallen, Helv. Phys. Acta **31**, 173 (1958).